J|A|C|S ARTICLES

Published on Web 02/03/2010

Transient Optical Studies of Interfacial Charge Transfer at Nanostructured Metal Oxide/PbS Quantum Dot/Organic Hole Conductor Heterojunctions

Henry C. Leventis,[†] Flannan O'Mahony,[†] Javeed Akhtar,[‡] Mohammad Afzaal,[‡] Paul O'Brien,[‡] and Saif A. Haque*,[†]

Nanostructured Materials and Devices Group, Department of Chemistry, Imperial College London, SW7 2AZ, United Kingdom, and School of Chemistry and School of Materials, The University of Manchester, Oxford Road, Manchester, M13 9PL United Kingdom

Received October 29, 2009; E-mail: s.a.haque@imperial.ac.uk

Abstract: We report a transient absorption and luminescence study addressing the charge separation, recombination, and regeneration reactions at nanostructured metal oxide/PbS quantum dot/organic hole conductor heterojunctions. We show that yields of charge separation are significantly higher at PbS/SnO_2 interfaces relative to PbS/TiO_2 interfaces, and conclude that this behavior is a result of the ca. 300−500 meV lower conduction band edge in SnO_2 as compared to TiO_2. We also report a correlation between the PbS particle size and the yield of charge separation at PbS/SnO_2 interfaces, with a smaller PbS particle radius resulting a higher yield of charge separation. Finally we investigated the regeneration of the photooxidized PbS by an organic hole transporting material, namely, *spiro*-OMeTAD. The overall *spiro*-OMeTAD$^+$ yield is found to be 27% at a SnO_2/PbS (∼3 nm diameter)/*spiro*-OMeTAD heterojunction. The addition of a lithium salt was found to raise the overall *spiro*-OMeTAD$^+$ yield from its initial value of 27% (where no Li^+ is present) to 50%. We believe this to be a result of an increase in the primary charge injection yield to near unity as the SnO_2 conduction band is lowered (with increasing [Li^+]), increasing the driving force for electron injection. The present findings are discussed with relevance to the design of PbS-sensitized metal oxide layers for DSSCs.

Introduction

Nanocomposites of inorganic and organic semiconductor materials are currently attracting significant interest for the development in range of electronic device applications such as light emitting diodes and solar cells.[1−4] A configuration of particular interest is the dye-sensitized nanocrystalline semiconductor solar cell (DSSC), where typically a mesoporous metal oxide film is coated with a monolayer of a light harvesting dye. The current state of the art DSSCs are based upon organometallic ruthenium dyes, although more recently there has been extensive interest in the use of alternative sensitsers such as conjugated polymers,[5] organic pigments,[6] and inorganic nanocrystals such as quantum dots (vide infra).

Interest in the use of semiconductor nanocrystals as sensitizers in DSSCs has been driven by the potential of extending the light-harvesting, and thus the current generating ability, of such devices into the near-IR region of the solar spectrum. These nanostructures can be incorporated either via attachment of colloidal QDs to the mesoporous metal oxide (MO) electrode by means of a bifunctional linker molecule,[4,7,8] or by in situ growth of semiconductor nanocrystal layers by chemical bath deposition techniques such as SILAR (successive ionic layer adsorption and reaction).[9−11] A variety of nanocrystal materials (including CdS, CdSe, and PbS), attached using either of these methodologies, have been investigated as light absorbers in liquid electrolyte and solid-state DSSCs. It is of interest that superior device performance has, to date, been realized using SILAR deposition, where power conversion efficiencies of up to 4.22% (under AM1.5 illumination) have been reported.[12] This observation is despite the fact that nanocrystals grown by this method have broad size distributions and, in most cases, no

[†] Imperial College London.
[‡] The University of Manchester.

(1) Haque, S. A.; Koops, S.; Tokmoldin, N.; Durrant, J. R.; Huang, J. S.; Bradley, D. D. C.; Palomares, E. *Adv. Mater.* **2007**, *19*, 683–687.
(2) Ravirajan, P.; Bradley, D. D. C.; Nelson, J.; Haque, S. A.; Durrant, J. R.; Smit, H. J. P.; Kroon, J. M. *Appl. Phys. Lett.* **2005**, *86*, 143101.
(3) Milliron, D. J.; Gur, I.; Alivisatos, A. P. *MRS Bull.* **2005**, *30*, 41–44.
(4) Kamat, P. V. *J. Phys. Chem. C* **2008**, *112*, 18737–18753.
(5) Zhu, R.; Jiang, C. Y.; Liu, B.; Ramakrishna, S. *Adv. Mater.* **2009**, *21*, 994–1000.
(6) Hagberg, D. P.; Yum, J. H.; Lee, H.; De Angelis, F.; Marinado, T.; Karlsson, K. M.; Humphry-Baker, R.; Sun, L. C.; Hagfeldt, A.; Gratzel, M.; Nazeeruddin, M. K. *J. Am. Chem. Soc.* **2008**, *130*, 6259–6266.
(7) Lee, H. J.; Yum, J. H.; Leventis, H. C.; Zakeeruddin, S. M.; Haque, S. A.; Chen, P.; Seok, S. I.; Grazel, M.; Nazeeruddin, M. K. *J. Phys. Chem. C* **2008**, *112*, 11600–11608.
(8) Leschkies, K. S.; Divakar, R.; Basu, J.; Enache-Pommer, E.; Boercker, J. E.; Carter, C. B.; Kortshagen, U. R.; Norris, D. J.; Aydil, E. S. *Nano Lett.* **2007**, *7*, 1793–1798.
(9) Lee, H. J.; Leventis, H. C.; Moon, S. J.; Chen, P.; Ito, S.; Haque, S. A.; Torres, T.; Nüesch, F.; Geiger, T.; Zakeeruddin, S. M.; Grätzel, M.; Nazeeruddin, M. K. *Adv. Funct. Mater.* **2009**, *19*, 1–8.
(10) Plass, R.; Pelet, S.; Krueger, J.; Gratzel, M.; Bach, U. *J. Phys. Chem. B* **2002**, *106*, 7578–7580.
(11) Vogel, R.; Hoyer, P.; Weller, H. *J. Phys. Chem.* **1994**, *98*, 3183–3188.
(12) Lee, Y. L.; Lo, Y. S. *Adv. Funct. Mater.* **2009**, *19*, 604–609.

surface passivation; indeed the lack of surface passivating (insulating) layers may be especially important.

Lead sulfide quantum dots are attractive candidates as light absorbers in solar cells as they typically exhibit narrow bandgaps, high extinction coefficients, and their absorption onset can be tuned over a large wavelength range: from that of bulk PbS (0.41 eV),[13] all the way into the visible region of the solar spectrum. Such behavior arises from the strong quantum confinement of charge carriers in the material, which can be several times stronger in lead-based QDs than in most III−V or II−VI semiconductors.[14,15] Recent studies have addressed the use of narrow band gap sensitizers, such as PbS quantum dots, in DSSCs. For example it was shown recently that, while it is possible to achieve current generation from the absorption of IR photons (in the 700−800 nm region) using SILAR-grown PbS sensitizers, IPCE values are low (<10%) at these wavelengths.[9] More specifically, it was shown that the yield of panchromatic current generation in solid state DSSCs is significantly lower with the use of PbS sensitizers compared to ruthenium Z907 dyes.[9] Other studies have also reported the application of narrow bandgap semiconductor nanocrystals (including those made from Sb_2S_3,[11,16] InAs,[17] PbS,[11,18,19] Bi_2S_3,[11,20] and InP[21]) as light absorbers in DSSCs, although as yet device efficiencies are significantly lower than those seen using conventional sensitizer dyes. Moreover, these findings could be an indication that interfacial charge separation yields are not optimized in these systems. To date, very few studies have examined the mechanisms of charge injection, regeneration, and recombination at PbS/metal oxide interfaces.

In Figure 1 we show the key interfacial charge transfer processes occurring at a typical metal oxide/PbS/HTM (hole transporting material) interface. Optical excitation of the light absorbing species results in electron injection from photoexcited state of the sensitizer into the conduction band of the metal oxide (reaction 1). The regeneration of oxidized light absorber is achieved by electron donation from the hole transporting material (reaction 2). Efficient operation of the DSSC device requires a high yield of interfacial charge separation and the minimization of recombination losses between the photoinjected electrons in the metal oxide and the oxidized PbS (reaction 3), and the oxidized HTM (reaction 4). Therefore, optimal device performance depends critically on the ability to control the relative rates of these two interfacial charge transfer processes. It is particularly apposite to use narrow bandgap semiconductors in DSSCs in trying to understand which of the underlying parameters determine the rates and yields of reactions 1 and 2. The reduction in sensitizer bandgap is expected to lower the thermodynamic driving force (ΔG) for both the electron injection process at the metal oxide/QD interface, and the regeneration process occurring at the QD/HTM interface.

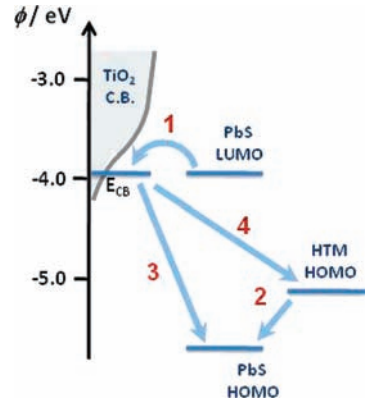

Figure 1. Simplified illustration of the redox process in operation at a typical metal oxide/PbS QD/HTM interface, following photoexcitation of PbS. Arrows indicate the direction of electron transfer for (1) photoinduced electron injection, (2) regeneration of QD-localized holes, (3) recombination between conduction band electrons in the metal oxide and PbS-localized holes, and (4) recombination between conduction band electrons and the oxidized HTM species. Estimates of band edge positions (vs vacuum) are provided, for PbS QDs with a first excitonic maximum at ca. 780 nm.

In this paper, we focus on the interfacial charge transfer processes at nanocrystalline metal oxide/PbS/organic HTM interfaces. We employ time-resolved transient absorption and luminescence spectroscopies to study the charge separation, recombination, and regeneration processes at these heterojunctions. In particular, we examine the influence of free energy driving force upon the primary charge separation step in colloidal PbS quantum dot-sensitized metal oxide films. The modulation of ΔG is achieved by varying the conduction band energetic of both the metal oxide and the PbS quantum dot, by changing the metal oxide type and PbS particle size, respectively. While factors such as the QD size-dependence of electron injection[18,22] and the distance-dependence of charge transfer yield[19,23] have been investigated for nanocrystal sensitizers, the impact of adjusting the energy of electron-accepting states within the metal oxide has largely escaped attention. In this work, we show that that yields of charge separation are significantly higher at PbS/SnO_2 interfaces relative to PbS/TiO_2 interfaces, and conclude that this behavior is a result of the ca. 300−500 meV[24,25] lower conduction band edge in SnO_2 as compared to TiO_2. In essence, the SnO_2 conduction band structure is more compatible with electron injection from PbS QDs than that of TiO_2. Finally, an organic HTM is included so as to study the factors influencing the overall yield and lifetime of charge separation across the metal oxide/HTM interface, and the impact of the incorporation of ionic additives within the HTM (intended to modulate the conduction band energy of the metal oxide

(13) McDonald, S. A.; Konstantatos, G.; Zhang, S. G.; Cyr, P. W.; Klem, E. J. D.; Levina, L.; Sargent, E. H. *Nat. Mater.* **2005**, *4*, 138–U14.
(14) Kang, I.; Wise, F. W. *J. Opt. Soc. Am. B* **1997**, *14*, 1632–1646.
(15) Wise, F. W. *Acc. Chem. Res.* **2000**, *33*, 773–780.
(16) Itzhaik, Y.; Niitsoo, O.; Page, M.; Hodes, G. *J. Phys. Chem. C* **2009**, *113*, 4254–4256.
(17) Yu, P. R.; Zhu, K.; Norman, A. G.; Ferrere, S.; Frank, A. J.; Nozik, A. J. *J. Phys. Chem. B* **2006**, *110*, 25451–25454.
(18) Hyun, B. R.; Zhong, Y. W.; Bartnik, A. C.; Sun, L. F.; Abruna, H. D.; Wise, F. W.; Goodreau, J. D.; Matthews, J. R.; Leslie, T. M.; Borrelli, N. F. *ACS Nano* **2008**, *2*, 2206–2212.
(19) Yang, S. M.; Wang, Z. S.; Huang, C. H. *Synth. Met.* **2001**, *123*, 267–272.
(20) Peter, L. M.; Wijayantha, K. G. U.; Riley, D. J.; Waggett, J. P. *J. Phys. Chem. B* **2003**, *107*, 8378–8381.
(21) Zaban, A.; Micic, O. I.; Gregg, B. A.; Nozik, A. J. *Langmuir* **1998**, *14*, 3153–3156.
(22) Robel, I.; Kuno, M.; Kamat, P. V. *J. Am. Chem. Soc.* **2007**, *129*, 4136–4137.
(23) Robel, I.; Subramanian, V.; Kuno, M.; Kamat, P. V. *J. Am. Chem. Soc.* **2006**, *128*, 2385–2393.
(24) Anderson, N. A.; Lian, T. Q. *Annu. Rev. Phys. Chem.* **2005**, *56*, 491–519.
(25) Green, A. N. M.; Palomares, E.; Haque, S. A.; Kroon, J. M.; Durrant, J. R. *J. Phys. Chem. B* **2005**, *109*, 12525–12533.

substrate) is also investigated. The present findings are discussed with relevance to the design of PbS-sensitized metal oxide layers for DSSCs.

Experimental Section

A typical experiment for making PbS nanoparticles involves a reaction between PbO (0.90 g, 3.75 mmol) dissolved in 12.5 mL of olive oil (see Supporting Information) along with 1 mL of octadecene and 1 mL of oleic acid in a 100 mL of three-necked flask equipped with a condenser and thermometer. The third neck of the flask was closed with septum. Prior to placing it under vacuum, the flask was flushed with N_2 and gradually heated to 150 °C for 1 h. The flask was again filled with N_2 and the injection temperature was adjusted at 60 °C. In a second two-neck 100 mL flask, bis(trimethylsilyl)sulfide (TMS) (100 μL, 0.93 mmol) diluted with 2 mL of olive oil and 0.5 mL of octadecene was swiftly injected into the first flask using a syringe. The color of contents changed immediately from red-brown to dark brown/black. The reaction was finally quenched with 20 mL of anhydrous acetone, and the mixture was centrifuged for 10 min. The supernatant was discarded, and the precipitated nanoparticles were dispersed in dry toluene (5 mL) and reprecipitated by adding anhydrous acetone to wash off any excess solvent. By varying the growth time from 10 to 180 s, different size PbS nanoparticles could be effectively prepared.

Steady-state absorption spectroscopy of the QDs was performed using a Perkin-Elmer Lambda 750 UV−vis−n-IR spectrometer, and it was established that the QDs had first excitonic maxima at ca. 730, 780, 980, 1200, and 1350 nm; we therefore infer the following mean QD sizes for the respective samples: 2.8 ± 0.2, 3.0 ± 0.2, 3.7 ± 0.3, 4.6 ± 0.4, and 5.1 ± 0.4 nm.[26] The preparation of pastes of 20 nm TiO_2 nanoparticles were carried out as described previously.[7] SnO_2 (15 nm)[25] and ZrO_2 (20−30 nm) nanoparticle pastes were also prepared using previously published methods. Mesoporous metal oxide films were prepared on F-doped SnO_2 conducting glass (sheet resistance 15 Ωm^{-2}), by doctor blading and subsequent sintering at 450 °C, and the resulting films were found (by profilometry) to be between 2 and 2.5 μm in thickness (ca. 5.5 μm for ZrO_2 films). Sensitization of mesoporous metal oxide films with colloidal PbS was performed by first immersing the substrates overnight in a solution of 0.1 M mercaptopropionic acid (Sigma-Aldrich, ≥ 99%) in ethanol, and then washing them with excess ethanol. Films were then immersed overnight in solutions of PbS QDs in toluene, and then were washed to remove QDs not directly attached to metal oxide surface.

Spin coating of *spiro*-OMeTAD (2,2′,7,7′-tetrakis-(*N*,*N*-di-*p*-methoxyphenyl-amine)-9,9′-*spiro*bifluorene, Covion), was for most experiments, performed using a 0.1 M solution in chlorobenzene. The HTM solution was allowed to remain on the substrate for 1 min before spin-coating was performed at 2000 rpm (all solutions were filtered before use). The additives lithium bis(trifluoromethane-)sulfonamide (99.5%, Aldrich) and distilled *tert*-butylpyridine were included in some experiments, as described in the text. PbS growth using SILAR (successive ionic absorption and reaction) was carried out as described previously;[9] the spin coating solution in this case contained Li^+ and *tert*-butylpyridine additives and was partially oxidized using the oxidant $N(p\text{-}C_6H_4Br)_3SbCl_6$.[9]

Investigation of the primary charge separation process at PbS/metal oxide interfaces was carried out using two methodologies: (1) Comparison of photoluminescence decay dynamics, by means of time correlated single photon counting (TCSPC), employing a Jobin Yvon IBH Fluorocube laser system. Excitation was performed at 467 nm (1 MHz, 80 μW cm^{-2} average intensity, instrument response 250 ps fwhm), with a 695 nm long pass filter for emission detection. The laser repetition rate was reduced when long (>100 ns) emission lifetimes were studied. (2) Transient absorption studies, which were carried out as described previously.[27] Sample excitation was carried out at 500 nm with pulses from a nitrogen laser-pumped dye laser (<1 ns pulse duration, 4 Hz) with pulse energies of 75 μJ cm^{-2} unless stated. Resulting photoinduced changes in optical density were probed using a 100 W tungsten lamp, with 20 nm bandwidth monochromators before and after the sample. The detection systems used were home-built, and based on Si and $In_xGa_{1-x}As$ photodiodes (employed for measurements below and above 1000 nm, respectively); changes were observed and recorded with the aid of a Tektronix TDS 1012 oscilloscope.

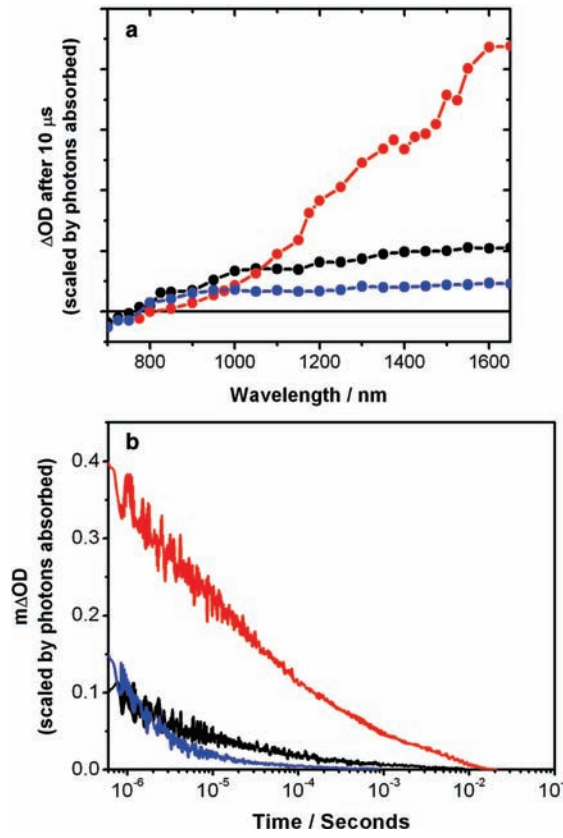

Figure 2. (a) Transient spectra observed 10 μs following photoexcitation at 500 nm for TiO_2/PbS (black), SnO_2/PbS (red), and ZrO_2/PbS (blue) architectures. Values of ΔOD have been scaled by the fraction of photons absorbed at the pump wavelength. Data are shown for QDs having a first excitonic maximum at 730 nm. (b) Transient kinetics, probing PbS-localized holes (at 1600 nm) in metal oxide/PbS QD architectures. Data using mesoporous TiO_2 (black trace) are compared with those obtained when SnO_2 (red trace) and ZrO_2 films (blue trace) were used. Values of ΔOD have been scaled by the fraction of photons absorbed at the pump wavelength, and samples were excited at 500 nm (pump intensity 65 $\mu J\ cm^{-2}$). Data are shown for QDs having a first excitonic absorption maximum at 730 nm.

Results and Discussion

We consider first the charge separation and recombination processes at PbS/metal oxide interfaces, by comparing the use of three different metal oxide substrates: SnO_2, TiO_2 and ZrO_2. As described in the experimental section, oleic acid was employed as the passivating ligand in the synthesis of PbS QDs. Pulsed optical excitation of the PbS-sensitized metal oxide films resulted in the appearance of a broad, long-lived, positive band above *ca.* 1000 nm (Figure 2a), which extend toward the near-infrared. Similar long-lived features have been reported in the

(26) Cademartiri, L.; Montanari, E.; Calestani, G.; Migliori, A.; Guagliardi, A.; Ozin, G. A. *J. Am. Chem. Soc.* **2006**, *128*, 10337–10346.

(27) Haque, S. A.; Tachibana, Y.; Willis, R. L.; Moser, J. E.; Gratzel, M.; Klug, D. R.; Durrant, J. R. *J. Phys. Chem. B* **2000**, *104*, 538–547.

literature,[7,9,28] and attributed to nanocrystal-localized holes which are formed as a result of photoinduced electron injection into metal oxide conduction bands.[7] It is apparent that the broad positive feature is seen with the use of all three metal oxides (SnO_2, TiO_2 and ZrO_2). Furthermore, it is evident from these data that the yield of PbS-localized holes is significantly larger (at 10 μs) when SnO_2 films are used in place of TiO_2 films. The higher yield of photogenerated holes in the SnO_2 sensitized film is consistent with an increase in driving force for electron injection as a result of the ca. 300−500 meV[22,23] lower conduction band edge in SnO_2 as compared to TiO_2. It is pertinent to note that some charge separation is seen using mesoporous ZrO_2 (which has a sufficiently high conduction band to prohibit electron injection),[29,30] although the positive transient obtained using this architecture is extremely small in amplitude on long time scales (>10 μs).

The charge recombination reaction between photoinjected electrons in the metal oxide and the photooxidized PbS quantum dots (for the three different metal oxides) is studied in Figure 2b. These data were obtained by monitoring the decay at 1600 nm; they have also been scaled by the percentage of photons absorbed at 500 nm (the pump wavelength) to normalize for any differences in sensitization yield, and thus optical absorption. No rise in the transient signal is observed in our data, so we conclude that the electron injection process occurs on time scales shorter than the resolution of our equipment. It is evident from these data that the lifetimes of the charge-separated states are not dissimilar in the SnO_2 and TiO_2 systems, and that the yield of long-lived PbS-localized holes is up to five times larger when SnO_2 films are used. Examination of the transient absorption kinetics of the PbS/ZrO_2 architecture reveals the tail of a fast decay component; it is possible that this can be rationalized by taking into account the recombination of separated charges within individual quantum dots.[31] The signal appears larger that of the PbS/TiO_2 system on submicrosecond time scales, an observation which could indicate that the QD-localized hole is not the only species giving rise to a transient absorption feature in the near-IR, and that uninjected electrons may also have this property.

To determine the yield of electron injection from photoexcited PbS QDs into metal oxide conduction bands, we examined the quenching of the PbS band-edge emission using time-resolved photoluminescence spectroscopy. A PbS/ZrO_2 film was used as a control as its higher lying conduction band edge inhibits electron injection. Indeed, it is apparent that the PL dynamics of PbS anchored on ZrO_2 appear accelerated relative to oleic acid-capped PbS quantum dots in solution (Figure 3, inset). The emission dynamics of PbS QDs dispersed in toluene are compared before (τ = 1080 ns; a value which is in accord with those reported previously for PbS QDs in solution)[18] and after (τ = 2.28 ns) ligand exchange using aliphatic thiol ligands. It is not unreasonable to suppose that the passivating-ligand exchange process that is employed in the attachment of the QD to the metal oxide surface (replacing oleic acid ligands with thiols) may induce changes in the PL lifetime of PbS quantum dots.[32−34] A detailed understanding of the origins of these observations is beyond the scope of this paper; but will be addressed in our future work. However it is possible that the decrease in PL lifetime in PbS/ZrO_2 films, relative to oleic acid-capped PbS quantum dots in solution, may be due either to nonradiative recombination pathways competing more efficiently with the shallow-trap PL in PbS QDs as the surface passivation is disrupted, or to charge separation occurring within the quantum dot, resulting in PL quenching and charge separation at the QD surface. More detailed studies addressing the effect of capping ligands on the efficiency and lifetime of PbS photoluminescence are currently underway and will be reported in due course.

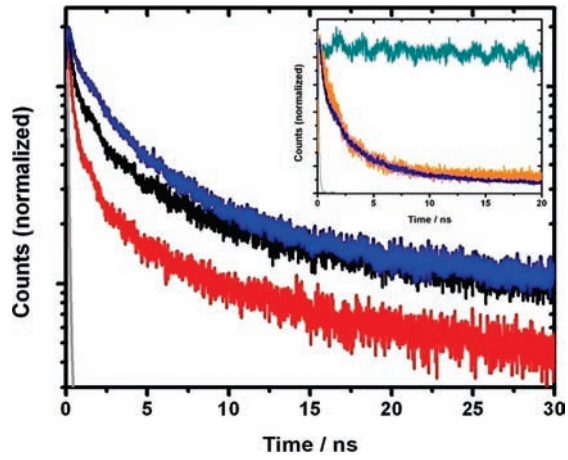

Figure 3. Normalized photoluminescence decay dynamics of the shallow trap emission of PbS QDs attached to ZrO_2 (blue trace), TiO_2 (black trace), and SnO_2 (red trace) nanoparticle films. Samples were excited at 467 nm, following which photons over 695 nm were collected. The system instrument response is shown in light gray, and is less than 250 ps. Inset: Normalized photoluminescence decay dynamics of PbS QDs dispersed in toluene before (green trace) and after (orange trace) the addition of a small amount of octanethiol. Data are compared to PbS QDs attached (by means of a thiol moiety) to a mesoporous ZrO_2 film (blue trace). Data are shown for QDs having a first excitonic absorption maximum at 730 nm.

It is clear that the PL lifetime decreases when QDs are bound to SnO_2 (τ = 0.42 ns) or TiO_2 (τ = 1.20 ns) films, when compared to the use of ZrO_2 (τ = 2.28 ns) substrates (Figure 3). We infer that electron injection occurs on the (sub)nanosecond time scale and is faster than the rate of trapping in these QDs. In addition, by comparison of the integrated areas of the respective traces, we conclude the yield of electron injection into nanostructured SnO_2 films to be at least ca. 59%, 3.5 times larger than that seen when TiO_2 is used (ca. 17%). This observation is in agreement with the transient absorption studies presented earlier, in which an analogous improvement in the yield of long-lived hole species on the QDs was observed with the use of SnO_2. It is therefore reasonable to conclude that the TiO_2 conduction band edge lies at too high an energy for efficient electron injection to occur from the PbS QDs employed here, and that (in this case at least) the use of SnO_2 is preferable for the achievement of high yields of interfacial charge separation. Furthermore, such agreement of TAS data (studying the yield of electron injection by means of comparing the concentrations of PbS-localized holes which are formed as a

(28) Tachibana, Y.; Umekita, K.; Otsuka, Y.; Kuwabata, S. *J. Phys. Chem. C* **2009**, *113*, 6852–6858.
(29) Haque, S. A.; Palomares, E.; Cho, B. M.; Green, A. N. M.; Hirata, N.; Klug, D. R.; Durrant, J. R. *J. Am. Chem. Soc.* **2005**, *127*, 3456–3462.
(30) Xu, Y.; Schoonen, M. A. A. *Am. Mineral.* **2000**, *85*, 543–556.
(31) Zhang, J.; Jiang, X. M. *J. Phys. Chem. B* **2008**, *112*, 9557–9560.
(32) Landes, C.; Burda, C.; Braun, M.; El-Sayed, M. A. *J. Phys. Chem. B* **2001**, *105*, 2981–2986.
(33) Liu, I. S.; Lo, H. H.; Chien, C. T.; Lin, Y. Y.; Chen, C. W.; Chen, Y. F.; Su, W. F.; Liou, S. C. *J. Mater. Chem.* **2008**, *18*, 675–682.
(34) Munro, A. M.; Ginger, D. S. *Nano Lett.* **2008**, *8*, 2585–2590.

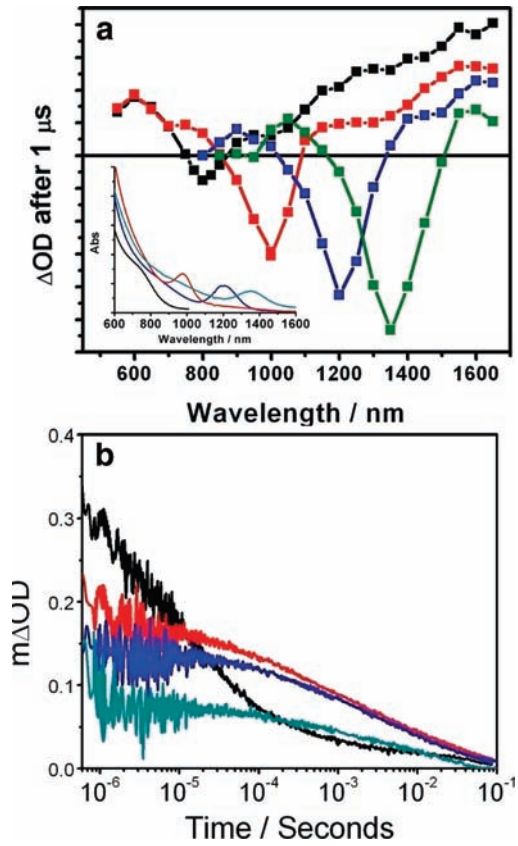

Figure 4. (a) Transient spectra (obtained 10 μs following photoexcitation) of SnO_2/PbS QD architectures using PbS-780 (black data), PbS-980 (red data), PbS-1200 (blue data), and PbS-1350 (green data) sensitizers. Samples were excited at 500 nm, using a pump energy of 90 μJ cm^{-2}. Values of ΔOD have been scaled by the fraction of photons absorbed at the pump wavelength. Steady-state absorption spectra of QD solutions in toluene are shown in the inset. (b) Transient kinetics, probed at 1600 nm, following photoexcitation (at 500 nm) of SnO_2/PbS QD architectures using PbS-780 (black trace), PbS-980 (red trace), PbS-1200 (blue trace), and PbS-1350 (green trace) sensitizers (pump energy 90 μJ cm^{-2}). Values of ΔOD have been scaled by the fraction of photons absorbed at the pump wavelength.

result) with PL quenching data (which study the fate of the emissive state in PbS QDs) appears to indicate that the PL quenching dynamics provides a good indication of the *overall* yield of photoinduced electron injection, from both emissive and nonemissive states. Our findings indicate that both of these processes are possible. It should be noted that our results seem to differ from those obtained by Hyun et al.,[18] whose studies of the fluorescence quenching of PbS QDs coupled to colloidal TiO_2 nanoparticles appear to demonstrate electron injection yields approaching unity for QDs with a first excitonic maximum below ca. 870 nm. We believe that this discrepancy could result from the use of colloidal PbS QDs in solution as a control for studies of PbS photoluminescence quenching by electron injection. Our investigations appear to indicate that QDs attached to ZrO_2 nanoparticles (by means of the same bifunctional linker species) serve as a more appropriate control for PL studies.

The transient spectra of SnO_2/PbS films, when four different sizes of colloidal PbS QD are used, having first excitonic maxima at ca. 780, 980, 1200, and 1350 nm (PbS-780, PbS-980, PbS-1200, and PbS-1350, respectively) are reported in Figure 4a. Samples were excited at 500 nm, and changes in optical density were ascertained 1 μs after photoexcitation. At smaller QD sizes, spectra appear increasingly blue-shifted, consistent with the shifts seen in steady-state absorption spectra. The profile of the positive transient is not dissimilar in all three cases. It is clear that the yield of PbS-localized holes (at 1 μs) reduces steadily as the QD size is raised (and their lowest unoccupied molecular orbital (LUMO) is lowered). The change in quantum confinement imparted by reducing the QD size serves to raise the LUMO (or the "1s"-like conduction band state of the QD), thus potentially increasing injection yields. The LUMO energy of QDs can be estimated using the following zeroth-order approximation of the effective-mass model:[9,35]

$$E_{\mathrm{LUMO}} = E_{\mathrm{CB}}(\mathrm{bulk}) + (E_{\mathrm{g}}(\mathrm{QD}) - E_{\mathrm{g}}(\mathrm{bulk}))\left(\frac{m_{\mathrm{h}}}{m_{\mathrm{h}} + m_{\mathrm{e}}}\right)$$

where E_{CB}(bulk) is the bulk conduction band energy (versus vacuum), E_{g}(QD) and E_{g}(bulk) are the QD and bulk bandgaps, and m_{h} and m_{e} are the effective hole and electron masses in the bulk semiconductor. Using literature values E_{VB}(bulk), E_{g}(bulk), m_{h}, and m_{e} in PbS,[13,36] we ascribe a LUMO energy of ca. -3.95 eV (relative to vacuum) for PbS QDs with a first excitonic absorption maximum at 780 nm, and a highest occupied molecular orbital (HOMO) level of ca. -5.54 eV. As electrons and holes have a similar effective mass in PbS, we believe that changes in confinement energy upon changing QD size should be evenly apportioned in shifting the HOMO and LUMO energies.

The bleach of the first excitonic absorption feature appears to decrease in amplitude for smaller QD sizes. It is possible that such bleaching occurs as a result of the presence of uninjected electrons on the PbS QDs, which decrease in number as the QD size is reduced, and electron injection becomes more energetically favorable. As the bleach decreases in amplitude, the positive transient grows concomitantly, consistent with the assignment of this feature to the absorption of PbS-localized holes.

The charge recombination dynamics between photoinjected electrons and the oxidized PbS QDs are shown, as a function of PbS particle size, in Figure 4b. It is apparent from these data that, while the yield of QD-localized holes improves with decreasing QD size (raising its LUMO energy), the lifetime of interfacial charge separation in PbS/SnO_2 architectures employing the smallest diameter quantum dots is shorter relative to the larger diameter quantum dots. This effect could, in part, be due to a reduction in the average distance between electrons and holes at the interface (which would serve to accelerate the recombination rate). It should be noted that, while other reports addressing the kinetics of charge recombination in QD-based solar cells exist in the literature,[28,37] we are in the process of conducting further studies on the PbS-sensitized DSSC architectures discussed herein and hope to present our findings in due course.

We consider next the PbS regeneration reaction at solid-state metal oxide/PbS/hole transporting material heterojunctions. In this work the *p*-type organic semiconductor *spiro*-OMeTAD (2,2′,7,7′-tetrakis-(*N*,*N*-di-*p*-methoxyphenyl-amine)-9,9′-*spiro*-bifluorene) is used as the hole transporting material. Figure 5 (main figure) compares the decay in the HTM^+ concentration

(35) Jasieniak, J.; Pacifico, J.; Signorini, R.; Chiasera, A.; Ferrari, M.; Martucci, A.; Mulvaney, P. *Adv. Funct. Mater.* **2007**, *17*, 1654–1662.
(36) Baskoutas, S.; Terzis, A. F. *Mater. Sci. Eng., B* **2008**, *147*, 280–283.
(37) Albero, J.; Martinez-Ferrero, E.; Ajuria, J.; Waldauf, C.; Pacios, R.; Palomares, E. *Phys. Chem. Chem. Phys.* **2009**, *11*, 9644–9647.

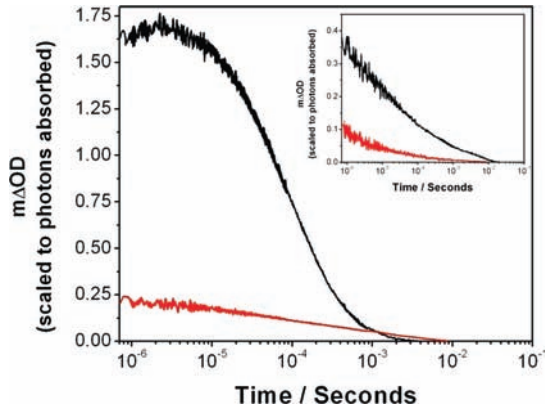

Figure 5. Transient kinetics, probing the (inset) PbS-localized hole absorption and (main figure) *spiro*-OMeTAD$^+$ cation absorption at 1600 nm, in the metal oxide/PbS (inset) and metal oxide/PbS/HTM (main figure) architectures. Data using mesoporous TiO_2 (red traces) are compared with those obtained when SnO_2 films are used (black traces). Samples were excited at 500 nm, using a pump energy of 74 μJ cm^{-2}. Values of ΔOD have been scaled by the fraction of photons absorbed at the pump wavelength. Data are shown for QDs having a first excitonic absorption maximum at 730 nm.

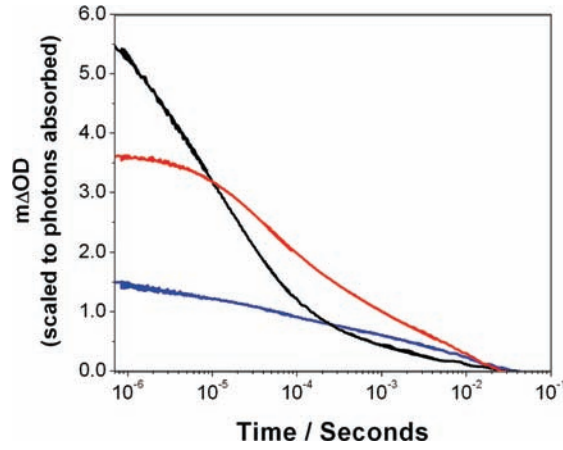

Figure 6. Transient kinetics probing the *spiro*-OMeTAD$^+$ cation absorption at 1600 nm in metal oxide/PbS/HTM architectures, where PbS nanocrystals were grown in situ using the SILAR method. Data using mesoporous SnO_2 (black trace) are compared with those obtained when TiO_2 films (red trace) and ZrO_2 films (blue trace) are used. Samples were excited at 500 nm, using a pump energy of 79 μJ cm^{-2}. Values of ΔOD have been scaled by the fraction of photons absorbed at the pump wavelength. For all three samples to have similar steady-state absorption profiles, different numbers of SILAR cycles were used: SnO_2 (three cycles); TiO_2 (five cycles); ZrO_2 (five cycles).

in SnO_2/PbS/HTM and TiO_2/PbS/HTM systems.[38] The data presented here follow the charge recombination between photoinjected electrons in the metal oxide and the oxidized *spiro*-OMeTAD; as before, they have been normalized to account for any differences in sensitization yield, in that the change in optical density has been scaled by the fraction of photons absorbed at 500 nm. These data appear to indicate that the overall *spiro*-OMeTAD$^+$ yield at 1 μs is ca. 8 times larger when SnO_2 is used; this difference supports our previous assertions as to this substrate acting more efficiently than TiO_2 in accepting electrons from photoexcited PbS QDs. It is also clear that the lifetime of the charge-separated state is ca. an order of magnitude faster when SnO_2 films are used. This is consistent with the studies of Green et al.,[25] who accounted for this behavior in liquid-electrolyte DSSCs by making reference to the 100-fold discrepancy between the electron diffusion coefficients in the respective metal oxide films.

It is also possible to grow semiconductor nanocrystals directly upon the surface of the mesoporous metal oxide film by use of the SILAR (successive ionic adsorption and reaction) technique. Performing multiple SILAR cycles leads to the growth of larger nanocrystals, which have an inhomogeneous size distribution, as seen by the lack of excitonic absorption features in steady-state absorption spectra of the sensitized films. Despite the broader PbS size distributions present in these systems, larger yields of HTM$^+$ generation were seen with SILAR-deposited PbS sensitizers (Figure 6) than were observed with the use of their colloidal counterparts. This could be a result of several factors. First, examination of the absorption spectra of our SILAR-sensitized films appears to indicate that these PbS nanocrystals are, in general, smaller than PbS QDs ($E_g \approx 1.6$ eV) studied previously, with E_g values approaching 2 eV. While the effect of nanocrystal size upon injection yield has already been examined, it should also be noted that an improvement in regeneration yield may also be possible as QD HOMO energies are lowered with increasing quantum confinement. In addition, SILAR-grown nanocrystals have no surface passivation (the colloidal PbS QDs used in this study are capped with oleic acid), a feature which could be conducive to the formation of an intimate contact at the QD/HTM interface (favorable for the efficient regeneration of PbS-localized holes). In addition, Figure 6 illustrates that higher HTM$^+$ yields (approaching unity per absorbed photon) can be achieved using mesoporous SnO_2, when compared to films structured from TiO_2 nanoparticles, although the lifetime of charge-separation appeared to be shorter in the former case (by ca. 1 order of magnitude). This is consistent with data presented earlier, where colloidal PbS QDs were used. There also appears to be a small amount of HTM$^+$ generation with the use of mesoporous ZrO_2 (where the conduction band is thought to be sufficiently high to prohibit electron injection from the PbS LUMO);[29] this possibly results from the regeneration of PbS-localized holes, which is able to compete with the recombination between electrons and holes separated within the nanocrystal layer.

Now attention is paid to the impact of ionic additives such as lithium salts upon the yield of charge generation in solid-state metal oxide/PbS/*spiro*-OMeTAD architectures. In particular, it is hoped that the poor yields of charge generation reported previously with the use of mesoporous TiO_2 can be improved by modulation of the energetics of the TiO_s conduction band. Previous studies have demonstrated that the presence of lithium additives in liquid electrolyte DSSCs employing dye sensitizers

(38) The oxidized form of *spiro*-OMeTAD is known to have a strong, broad absorption band in the near-IR region (peaking beyond 1400 nm, Plass, R.; Pelet, S.; Krueger, J.; Grätzel, M.; Bach, U. *J. Phys. Chem. B* **2002**, *106*, 75787580). It is possible to probe the HTM$^+$ species at 1600 nm as the changes in absorbance resulting from its formation are much larger than those seen for the PbS$^+$ species, and thus it can be studied virtually in isolation from the influence of the signal arising from residual PbS-localized holes. For oxidized *spiro*-OMeTAD, we have obtained a value of ε (1600 nm) = 22800 M^{-1} cm^{-1}.; this was achieved by using a literature value of ε (520 nm) = 18700 M^{-1} cm^{-1} (Bach, U.; Tachibana, Y.; Moser, J. E.; Haque, S. A.; Durrant, J.; Grätzel, M. R.; Klug, D. R. *J. Am. Chem. Soc.* **1999**, *121*, 7445–7446) and by considering the ratio of the optical absorbances at 520 and 1600 nm of *spiro*-OMeTAD which had been chemically oxidized in solution (via introduction of the N(PhBr)$_3^{+\cdot}$ species). The latter ratio was confirmed by comparing the heights of transient signals obtained at the two wavelengths in other experiments we have conducted on metal oxide/sensitizer/*spiro*-OMeTAD architectures (not discussed here)

can have a pronounced impact on the charge separation efficiencies yielded by these devices, either by their adsorption upon,[39−41] or intercalation within,[42] metal oxide films, or by ion binding to dye molecules.[43] One major consequence of the use of electrolytic additives is that the yield of photoinduced injection can be significantly improved by increasing the Lewis acidity of the electrolyte (which serves to lower the TiO_2 conduction band edge by electrostatic interaction); this can have a significant impact upon device photocurrent.[40] Here, we investigate whether similar effects can be seen with the use of PbS quantum dot sensitizers. Previously we have described how imparting a good energetic overlap between the quantum dot and metal oxide conduction bands can be critical to the achievement of high yields of charge photogeneration at QD/metal oxide interfaces. It therefore seems reasonable to infer that modulation of the metal oxide conduction band energy using Li^+ additives may be an attractive means of improving charge separation yields in DSSCs employing narrow-bandgap sensitizers such as PbS quantum dots.

We have already shown that the use of SnO_2 substrates, which have a lower conduction band energy than those constructed from TiO_2, can lead to significant improvements in charge photogeneration in the metal oxide/PbS/*spiro*-OMeTAD DSSC architecture. The effect of raising the lithium concentration for the SnO_2/PbS/HTM architecture can be seen by examination of Figure 7a. Low concentrations of lithium salt serve to raise the overall *spiro*-OMeTAD$^+$ yield from its initial value of 27% (where no Li^+ is present) to 50%, after which no additional improvement is seen. We believe this to be primarily because of an increase in the injection yield from ca. 59% (no Li^+ is present), to near unity as the SnO_2 conduction band is lowered (with higher Li^+), increasing the driving force for electron injection. It therefore appears that the limiting factor in achieving efficient charge separation in SnO_2/PbS/HTM architectures is the ability to achieve efficient regeneration of PbS-localized holes by the HTM (we estimate the regeneration yield to be ca. 50%). The apparent difficulties associated with the regeneration of PbS-localized holes, despite the provision of what appears to be a large driving force (the energy offset between the nominal QD HOMO level and that of the HTM), are striking, and could be due to a range of factors, such as the morphology of PbS/HTM interfaces (in particular, the retardation of charge transfer by bulky passivating ligands on the QD surface), local electrostatic effects, or the presence of sub-bandgap hole traps within the QD. These hole traps may be as a result of intrinsic defects, such as metal vacancies,[44,45] or may be formed upon the ligand exchange used to bind the QDs to the metal oxide surface. While the latter of these proposals has been used in our earlier rationalizations of experimental data, we remain in the process of investigating whether charge trapping processes are critical in limiting the charge collection efficiency of these devices.

Also shown in Figure 7a is the effect on the *spiro*-OMeTAD$^+$ generation yield of increasing [Li^+] in the TiO_2/PbS/HTM arrangement. It is clear that it is possible to improve the charge separation in these architectures; we believe this effect to result in the most part from the improvement in electron injection yield as the TiO_2 conduction band is shifted downward. This correlates well with time-resolved PL studies shown in Figure 7b, which show a considerable reduction in PL lifetime (and therefore injection efficiency) using the "optimized" Li^+ concentration determined from Figure 7a. However, even using this optimized concentration of lithium additive, overall yields of charge separation were almost 25% lower than in the optimized SnO_2/PbS/HTM architecture.

In summary, we have employed transient optical spectroscopy to study the charge transfer processes at metal oxide/PbS

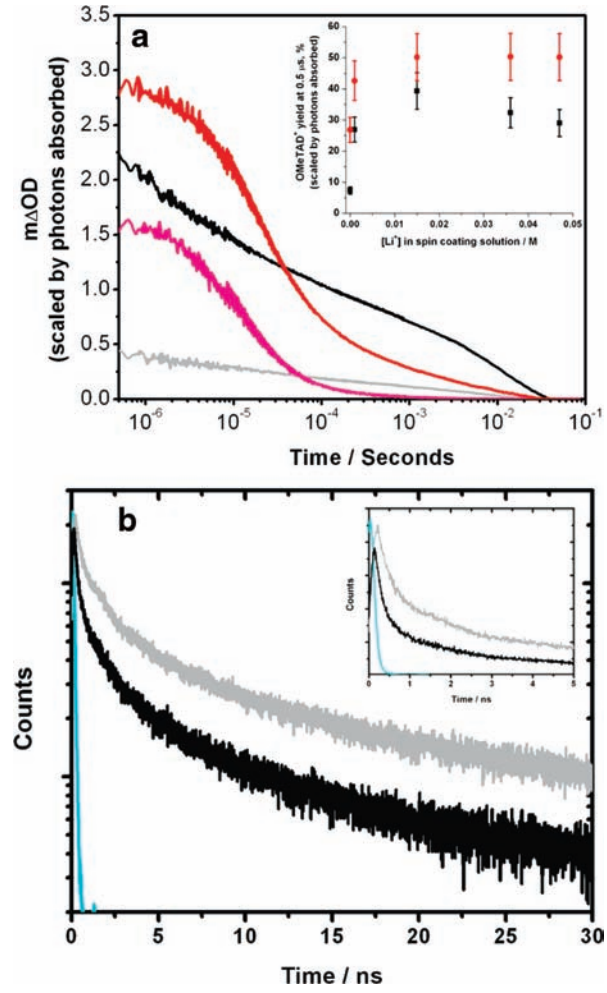

Figure 7. (a) Transient absorption kinetics, probing the *spiro*-OMeTAD$^+$ cation band at 1600 nm following photoexcitation of PbS QDs in TiO_2/PbS/*spiro*-OMeTAD (black and gray traces) and SnO_2/PbS/*spiro*-OMeTAD architectures (red and pink traces) at 500 nm (pump energy 65 μJ cm^{-2}). Pink and gray traces illustrate the impact of the inclusion of 16 mM lithium salt and 19 mM *tert*-butylpyridine in the spin-coating solution. Inset: Overall yield (at 0.5 μs) of *spiro*-OMeTAD$^+$ cations per absorbed photon, as a function of the concentration of lithium salt in the spin-coating solution (also containing 19 mM *tert*-butylpyridine), using TiO_2 (black data) and SnO_2 (red data) substrates. Data are shown for QDs having a first excitonic absorption maximum at 730 nm. (b) Time-resolved photoluminescence dynamics (normalized to the percentage of photons absorbed at the pump wavelength) for TiO_2/PbS/*spiro*-OMeTAD architectures. Black traces illustrate the impact of the inclusion of 0.016 M lithium salt and 19 mM *tert*-butylpyridine in the spin coating solution. Light blue traces represent the instrument response of the TCSPC setup used for the measurements. Samples were excited at 467 nm, following which photons over 695 nm were collected. Data are shown for QDs having a first excitonic absorption maximum at 730 nm.

(39) Redmond, G.; Fitzmaurice, D. *J. Phys. Chem.* **1993**, *97*, 1426–1430.
(40) Koops, S. E.; O'Regan, B. C.; Barnes, P. R. F.; Durrant, J. R. *J. Am. Chem. Soc.* **2009**, *131*, 4808–4818.
(41) Kelly, C. A.; Farzad, F.; Thompson, D. W.; Stipkala, J. M.; Meyer, G. J. *Langmuir* **1999**, *15*, 7047–7054.
(42) Kopidakis, N.; Benkstein, K. D.; van de Lagemaat, J.; Frank, A. J. *J. Phys. Chem. B* **2003**, *107*, 11307–11315.
(43) Furube, A.; Katoh, R.; Hara, K.; Sato, T.; Murata, S.; Arakawa, H.; Tachiya, M. *J. Phys. Chem. B* **2005**, *109*, 16406–16414.
(44) Babentsov, V.; Sizov, F. *Opto-Electron. Rev.* **2008**, *16*, 208–225.
(45) Watkins, G. D. *J. Cryst. Growth* **1996**, *159*, 338–344.

quantum dot/organic hole conductor heterojunctions. In particular, we have demonstrated that significantly higher yields of the primary charge injection process at the metal oxide/QD interface can be achieved through the appropriate choice of metal oxide, namely by using SnO_2 in place of TiO_2, and by using small PbS QDs ($\leq$ca. 3 nm in diameter). In addition, it has been shown that it is possible to obtain higher yields of charge separation by lowering the metal oxide conduction band energy (and thus the thermodynamic driving force for electron injection) via the use of Li^+ additives. We have investigated the yield of regeneration of the photooxidized PbS by an organic hole transporting material at the metal oxide / PbS / spiro-OMeTAD heterojunction. Steps have also been taken towards understanding the mechanism of hole regeneration in solid-state QD-DSSC architectures.

Acknowledgment. We acknowledge the Engineering and Physical Sciences Research Council (EPSRC) for their financial support. We thank Xiaoe Li for preparing nanoparticle pastes. J.A. thanks the higher education commission of Pakistan (HEC) for a Ph.D. studentship. S.A.H thanks the Royal Society for a Royal Society University Research Fellowship (RSURF). This paper was submitted while P.O.B. was a Visiting Fellow at Magdalen College Oxford. P.O.B. thanks the President and Fellowship for this excellent opportunity.

Supporting Information Available: Composition of olive oil used in this study. This material is available free of charge via the Internet at http://pubs.acs.org.

JA909172P